

# Magneto-optical Kerr Effect Characterization of Uniform Nanocrystalline Fe<sub>3</sub>O<sub>4</sub> Monolayer Fabricated on Silicon Substrate Functionalized with Catechol Groups

*Daisuke Hojo,<sup>\*a</sup> Kazuya Z. Suzuki,<sup>a</sup> Shigemi Mizukami,<sup>a</sup> and Tadafumi Adschiri<sup>ab</sup>*

<sup>a</sup> Advanced Institute for Materials Research, Tohoku University, 2-1-1 Katahira Aoba-ku Sendai 980-8577, Japan

<sup>b</sup> Institute of Multidisciplinary Research for Advanced Materials, Tohoku University, Katahira 2-1-1 Aoba-ku, Sendai 980-8577, Japan

## Supporting Information

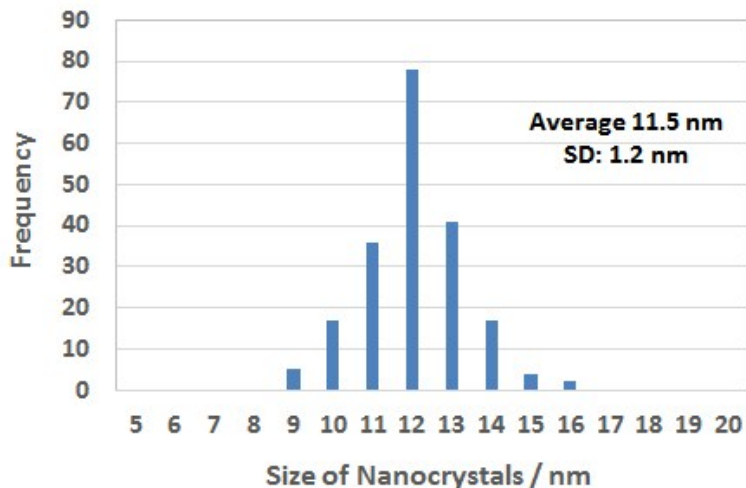
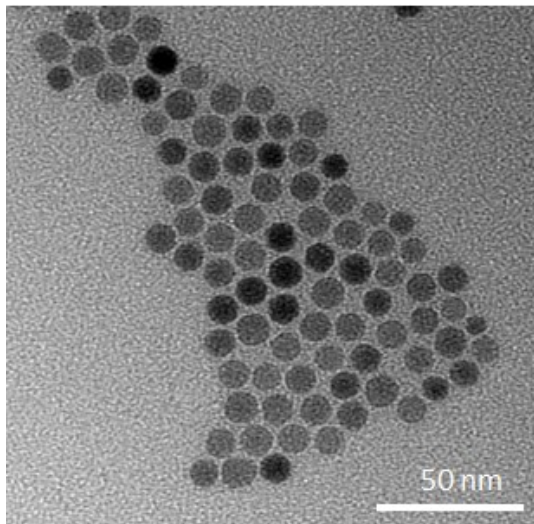


**Figure S1.** Transmission electron microscopy image of the  $\text{Fe}_3\text{O}_4$  nanocrystals.

### **S1. Sizes and size distributions of $\text{Fe}_3\text{O}_4$ nanocrystals synthesized in a mixture of oleic acid and oleylamine**

The transmission electron microscopy image of the synthesized  $\text{Fe}_3\text{O}_4$  nanocrystals is shown in Fig. S1. The sizes of the nanocrystals were evaluated to be  $13.4 \text{ nm} \pm 15\%$  from measurements of 200 randomly selected nanocrystals in the images. The size distribution is also shown in the histogram obtained from the 200 measurements.

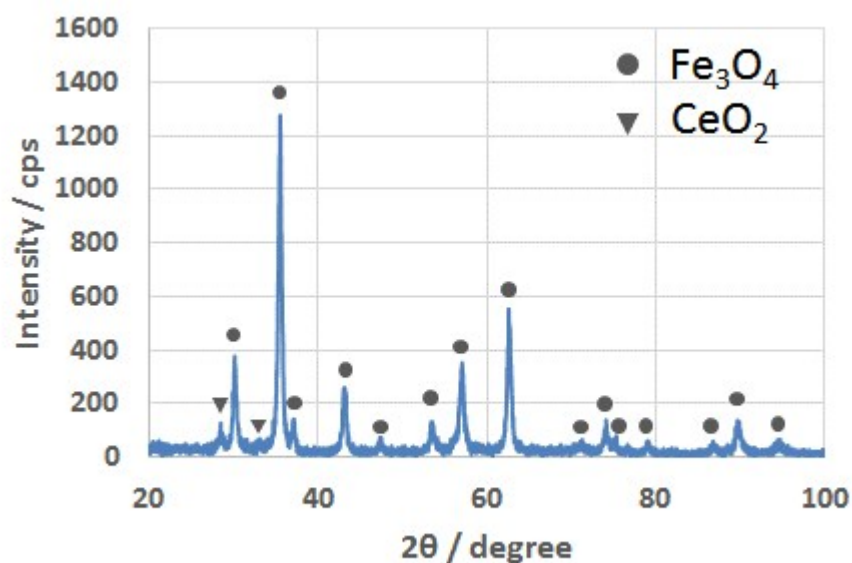


**Figure S2.** X-ray diffraction pattern of the Fe<sub>3</sub>O<sub>4</sub> nanocrystal powder after being freeze-dried.

## **S2. Crystal structure of magnetic nanocrystals synthesized in mixture of oleic acid and oleylamine**

The crystal structure of the nanocrystals synthesized in a mixture of oleic acid and oleylamine was investigated using X-ray diffraction analysis. The diffraction pattern associated with inverse-spinel Fe<sub>3</sub>O<sub>4</sub> (JCPDS No. 01-1111) was observed, as shown in Fig. S2. This result confirmed that Fe<sub>3</sub>O<sub>4</sub> nanocrystals were synthesized instead of those of  $\gamma$ -Fe<sub>2</sub>O<sub>3</sub>. The crystalline size as determined using Scherrer's equation was approximately 200 Å. This value is comparable to that determined from the transmission electron microscopy images of the nanocrystals, indicating that single-crystalline nanoparticles were obtained.

The peaks observed at 28.4° and 33.1° were attributable to the (111) and (002) planes of fluorite-like CeO<sub>2</sub> (JCPDS No. 81-0792). The peaks of the (133) and (115) planes of Fe<sub>3</sub>O<sub>4</sub>, which were observed at 47.1° and 57.1°, overlapped with those of the (022) and (113) planes of CeO<sub>2</sub>, respectively; this conclusion is based on the fact that the peak intensities were slightly higher than those determined from calculations. The CeO<sub>2</sub> nanocrystals were incorporated during the freeze-drying process, because CeO<sub>2</sub> nanocrystals had also been dried in the freeze dryer used for the Fe<sub>3</sub>O<sub>4</sub> nanocrystals.

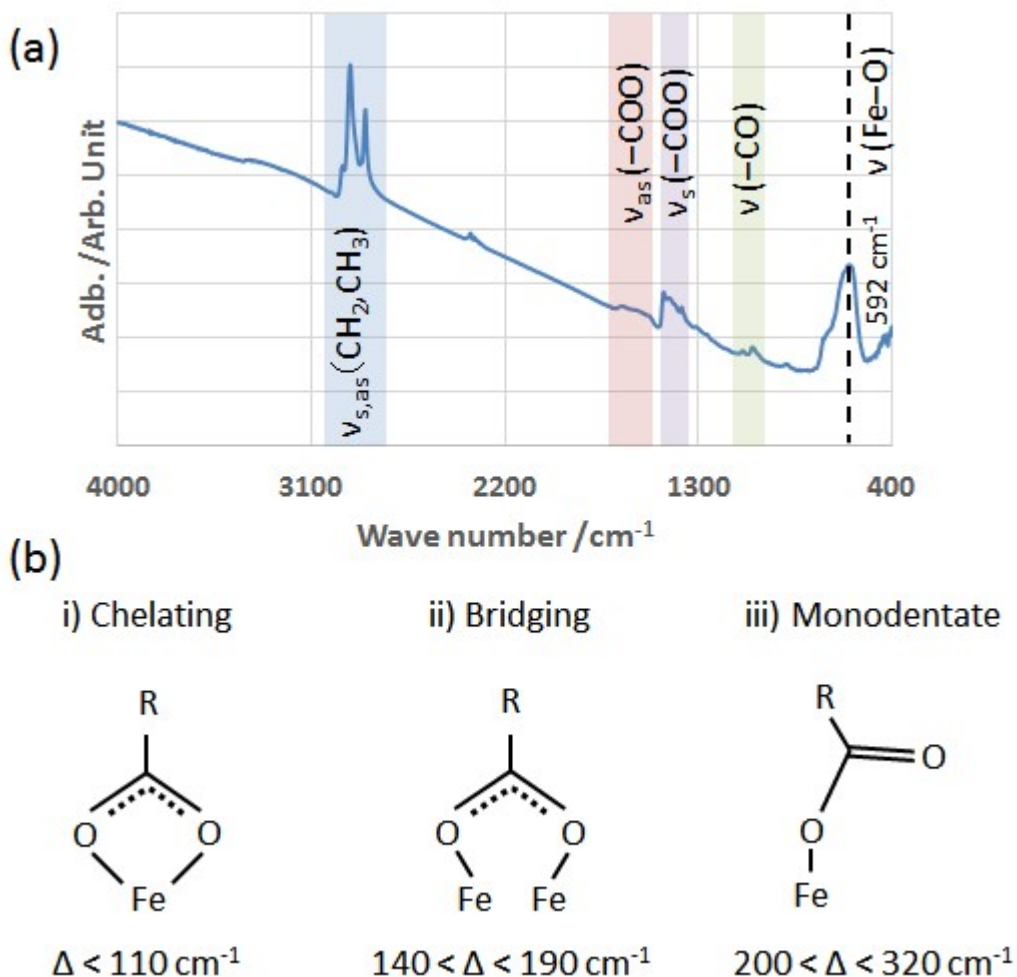


**Figure S3.** (a) Fourier transform infrared spectrum of the freeze-dried oleic-acid-modified  $\text{Fe}_3\text{O}_4$  nanocrystal powder. (b) Chemical structures of the surfaces of the  $\text{Fe}_3\text{O}_4$  nanocrystals modified by oleic acid. The carboxylate interaction can be categorized into three types, namely, those corresponding to a chelating bidentate, a bridging bidentate, and a monodentate interaction.

### S3. Chemical structure of oleic-acid-modified $\text{Fe}_3\text{O}_4$ nanocrystals

That the surfaces of the  $\text{Fe}_3\text{O}_4$  nanocrystals were modified by oleic acid was confirmed from their Fourier transform infrared (FTIR) spectrum, which is shown in Fig. S3(a). Strong bands corresponding to the symmetric and asymmetric stretching vibrations of the  $\text{CH}_2$  and  $\text{CH}_3$  groups of oleic acid were observed for wavenumbers of  $3000\text{--}2800\text{ cm}^{-1}$ .<sup>1-4</sup> Further, a typical peak related to Fe–O stretching vibrations was observed at  $592\text{ cm}^{-1}$ .<sup>2,3</sup> In addition, weak bands associated with the stretching vibration

modes of  $\text{-CO}$  were noticed at 1093 and 1049  $\text{cm}^{-1}$ .<sup>1-4</sup> A major peak associated with the symmetric stretching vibrations of the carboxylate group ( $\text{-COO}$ ) was seen at 1461  $\text{cm}^{-1}$ .<sup>1-5</sup> Finally, continuous bands assignable to the asymmetric stretching vibrations of the carboxylate group were observed at 1670–1520  $\text{cm}^{-1}$ .<sup>1-5</sup> These results confirmed that oleic acid was chemisorbed on the surfaces of the  $\text{Fe}_3\text{O}_4$  nanocrystals. Finally, the absence of the peak corresponding to the carboxyl group ( $\text{-COOH}$ ) of oleic acid at  $\sim 1710$   $\text{cm}^{-1}$  proved that the oleic acid was not physisorbed but chemisorbed on the surfaces.<sup>2,3</sup>

The chemical structures corresponding to the carboxylate interaction are shown in Fig. S3(b). Depending on the difference,  $\Delta$ , in the wavenumbers corresponding to the symmetric and asymmetric stretching vibration bands of the carboxylate group, the interaction of the carboxylate group with the metal ions can be categorized into different types.<sup>1-5</sup> The broad bands noticed at 1670–1520  $\text{cm}^{-1}$  indicate that carboxylate interactions related to a chelating bidentate, a bridging bidentate, and a monodentate interaction occurred on the surfaces of the  $\text{Fe}_3\text{O}_4$  nanocrystals.

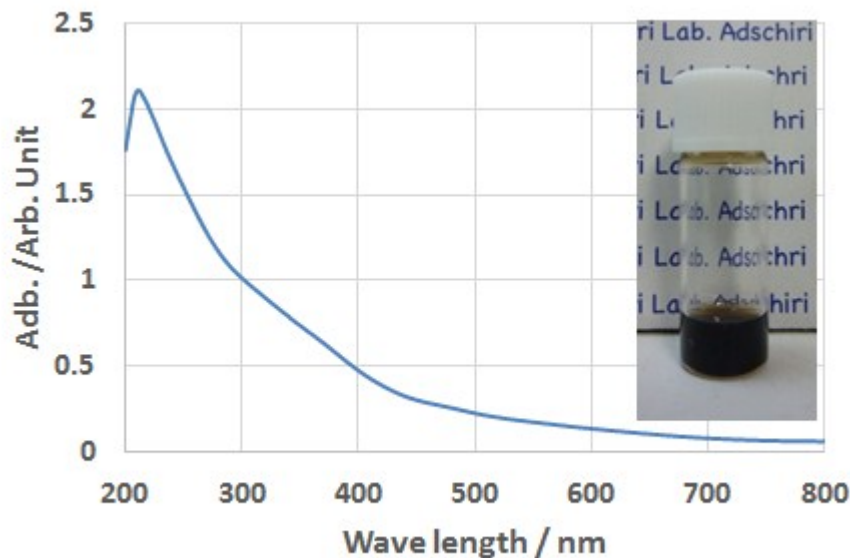


**Figure S4.** Ultraviolet-visible adsorption spectrum of the  $\text{Fe}_3\text{O}_4$  nanocrystals modified by oleic-acid dispersed in cyclohexane, and a photograph of the cyclohexane dispersion containing the oleic-acid-modified  $\text{Fe}_3\text{O}_4$  nanocrystals.

#### **S4. Ultraviolet-visible adsorption spectrum of oleic-acid-modified $\text{Fe}_3\text{O}_4$ nanocrystals**

The ultraviolet-visible (UV-vis) adsorption spectrum of the oleic-acid-modified  $\text{Fe}_3\text{O}_4$  nanocrystals dispersed in cyclohexane is shown in Fig. S4. A shoulder peak associated with ligand-to-metal charge transfer was observed at 300–400 nm in the spectrum.<sup>6</sup> This result is further evidence that the  $\text{Fe}_3\text{O}_4$  nanocrystals were modified by oleic acid. Finally, the cyclohexane dispersion containing the oleic-acid-modified  $\text{Fe}_3\text{O}_4$  nanocrystals was not cloudy, indicating that the nanocrystals had not agglomerated and caused extensive light scattering. The baseline of the UV-vis adsorption spectrum was also very small, owing to the low degree of light scattering.

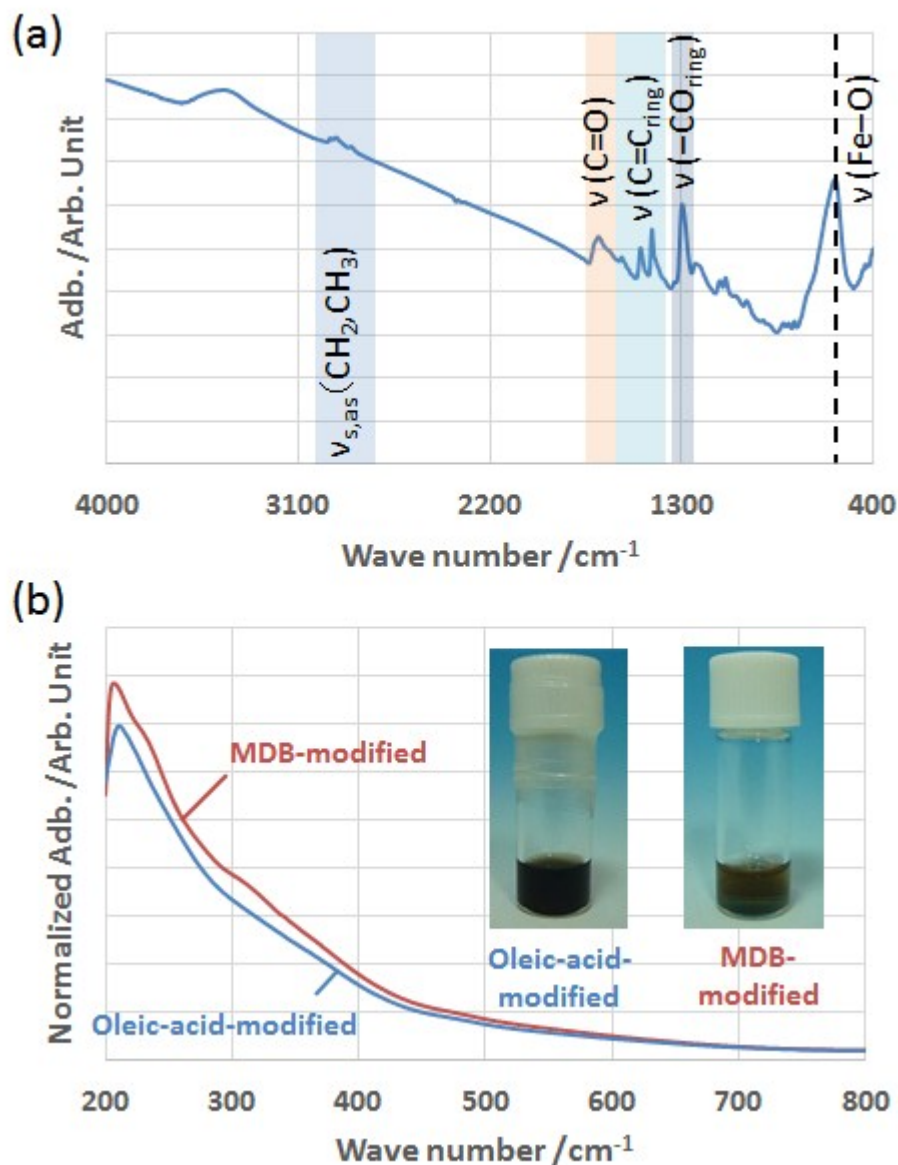


**Figure S5.** (a) Fourier-transform infrared spectrum of the freeze-dried methyl-3,4-dihydroxybenzoate (MDB)-modified  $\text{Fe}_3\text{O}_4$  nanocrystals after ligand-exchange reaction. (b) Ultraviolet-visible adsorption spectrum of the  $\text{Fe}_3\text{O}_4$  nanocrystals modified with MDB dispersed in ethanol, and a photograph of the ethanol dispersion containing the MDB-modified  $\text{Fe}_3\text{O}_4$  nanocrystals. The spectrum of the oleic-acid-modified  $\text{Fe}_3\text{O}_4$  nanocrystals dispersed in cyclohexane and a photograph of the cyclohexane dispersion containing the oleic-acid-modified  $\text{Fe}_3\text{O}_4$  nanocrystals are also displayed for comparison.

## S5. Ligand-exchange reactions on the surfaces of Fe<sub>3</sub>O<sub>4</sub> nanocrystals

To investigate whether chemical bonding was established between the Fe<sub>3</sub>O<sub>4</sub> nanocrystals and the catechol-functionalized substrates, MDB-modified Fe<sub>3</sub>O<sub>4</sub> nanocrystals were synthesized using a ligand-exchange technique from the oleic-acid-modified Fe<sub>3</sub>O<sub>4</sub> nanocrystals.

A solution containing MDB (25 mg) and ethanol (2 mL) was delivered dropwise into cyclohexane-dispersed oleic acid-modified Fe<sub>3</sub>O<sub>4</sub> nanocrystals (1 mL, 0.2 wt%); after introducing trimethylamine (200 mg), the mixture was stirred for 2 h at room temperature to effect the exchange of the catechol groups in MDB with the oleic acid ligands on the surfaces of the Fe<sub>3</sub>O<sub>4</sub> nanocrystals. The MDB-modified Fe<sub>3</sub>O<sub>4</sub> nanocrystals were separated from the residual MDB and oleic acid by centrifugation. The centrifuged product was then washed by centrifuging again with a mixture of cyclohexane (4.5 mL) and ethanol (4.5 mL). The washed product was dispersed in ethanol (2 mL, ~0.1 wt%) for UV-vis adsorption measurements. An FTIR spectrum of the sediments was collected after centrifugation and before dispersal in ethanol using an FTIR spectrometer.

That the surfaces of the Fe<sub>3</sub>O<sub>4</sub> nanocrystals were modified by MDB after the ligand-exchange reaction was confirmed from their FTIR spectrum, which is shown in Fig. S5(a). Weak bands corresponding to the symmetric and asymmetric stretching vibrations of the CH<sub>3</sub> group of MDB are observed for wavenumbers of 3000–2800 cm<sup>-1</sup>. A tiny peak associated with the symmetric vibrations of the CH<sub>2</sub> group is also observed, owing to residual ethanol, since ethanol was used for washing. A major peak associated with the stretching vibration modes of –CO<sub>ring</sub> of the catechol group in MDB is seen at 1294 cm<sup>-1</sup>.<sup>7</sup> The peaks assignable to the stretching ring vibrations of the catechol group are observed at 1437, 1492, and 1580 cm<sup>-1</sup>.<sup>7</sup> Further, the stretching vibration mode of C=O in MDB is observed at 1692 cm<sup>-1</sup>. Finally, the absence of the peaks corresponding to the carboxylate group (–COO) of oleic acid proves that oleic acid is no longer chemisorbed on the surface. These results confirm that MDB was chemisorbed on the surfaces of the Fe<sub>3</sub>O<sub>4</sub> nanocrystals instead of oleic acid.



The normalized UV-vis adsorption spectrum of the MDB-modified  $\text{Fe}_3\text{O}_4$  nanocrystals dispersed in ethanol is shown in Fig. S5(b). The UV-vis adsorption spectrum was normalized by the value at 800 nm, where we can assume no contribution to the adsorption by organic ligands, in order to compare the spectra of the MDB-modified with the oleic-acid-modified nanocrystals. The ethanol dispersion containing the MDB-modified  $\text{Fe}_3\text{O}_4$  nanocrystals is not cloudy in the photograph, indicating that the nanocrystals had not agglomerated and caused extensive light scattering. A shoulder peak is enhanced at 300–400 nm in the spectrum, compared with the spectrum of the oleic-acid-modified  $\text{Fe}_3\text{O}_4$  nanocrystals shown in Fig. S5(b). This result is not inconsistent with the result obtained by Yuen et al.,<sup>8</sup> because catechol ligands attach more strongly to the  $\text{Fe}_3\text{O}_4$  surfaces. Amstad et al. also confirmed a prominent peak located between 350 and 500 nm in a spectrum of nitrocatechol-modified magnetite.<sup>9</sup> Further, a broad peak is observed at 230–250 nm in the spectrum of the MDB-modified  $\text{Fe}_3\text{O}_4$  nanocrystals. We conclude that these peaks are associated with catechol ligand-to-metal charge transfer based on the results of the FTIR and UV-vis spectra.

Based on the foregoing discussion, we can rationalize that ligand exchange reactions occurred on the catechol-functionalized substrates as follows. Figure 3(d) in the main text shows the UV-vis reflectance spectrum of the  $\text{Fe}_3\text{O}_4$  nanocrystals formed on the functionalized and rinsed substrate. Compared with the spectrum of the  $\text{Fe}_3\text{O}_4$  nanocrystals fabricated on the nonfunctionalized and unrinsed substrate shown in Fig. 3(d), a broad peak is observed at 250 nm and the shoulder peak is enhanced at 300–500 nm in the spectrum. These two features are associated with catechol ligand-to-metal charge transfer, as discussed in the previous section. Thus, this reflectance spectrum confirms that local ligand-exchange reactions took place on the catechol-functionalized substrate, in which catechol groups became bound to the surfaces of the  $\text{Fe}_3\text{O}_4$  nanocrystals instead of oleic acid.

## REFERENCES

1. M. Taguchi, S. Takami, T. Naka, and T. Adschiri, *Cryst. Growth Des.* 2009, **9**, 5297–5303.
2. F. Yan, J. Li, J. Zhang, F. Liu, and W. Yang, *J. Nanopart. Res.* 2009, **11**, 289–296.
3. L. Zhang, R. He, and H.-C. Gu, *Appl. Surf. Sci.* 2006, **253**, 2611–2617.
4. Y. Ren, K. Iimura, and T. Kato, *Langmuir* 2001, **17**, 2688–2693.
5. K. Nakamoto, *Infrared and Raman Spectra of Inorganic and Coordination Compounds*; Wiley: New York, 1997.
6. N. Goswami, S. Chaudhuri, A. Giri, P. Lemmens, and S. K. Pal, *J. Phys. Chem. C* 2014, **118**, 23434–23442.
7. I. A. Janković, Z. V. Šaponjić, M. I. Ćomor, and J. M. Nedljković, *J. Phys. Chem. C* 2009, **113**, 12645–12652.
8. A. K. L. Yuen, G. A. Hutton, A. F. Masters, T. Maschmeyer, and S. K. Murthy, *J. Appl. Phys.* 2009, **105**, 07B317.
9. E. Amstad, A. U. Gehring, H. Fischer, V. V. Nagaiyanallur, G. Hähner, M. Textor, and E. Reimhult, *J. Phys. Chem. C* 2011, **115**, 683–691.